HHS Public Access

Author manuscript

J Am Chem Soc. Author manuscript; available in PMC 2021 March 11.

Published in final edited form as:

J Am Chem Soc. 2020 March 11; 142(10): 4631–4638. doi:10.1021/jacs.9b11266.

In-Situ Deactivation of Catechol-Containing Adhesive using Electrochemistry

Md. Saleh Akram Bhuiyan, **James D. Roland**, **Bo Liu**, **Max Reaume**, **Zhongtian Zhang**, **Jonathan D. Kelley**, **Bruce P. Lee***

Department of Biomedical Engineering, Michigan Technological University, Houghton, MI-49931, USA

Abstract

Marine mussels secret catechol-containing adhesive proteins that enable these organisms to bind to various surfaces underwater. Synthetic mimics of these proteins have been created to function as adhesives and coatings for a wide range of applications. Here, we demonstrated the use of in-situ electrical field stimulation to deactivate the adhesive property of catechol-containing adhesive that is in direct contact with a surface. Johnson-Kendall-Roberts (JKR) contact mechanics test was performed using a titanium (Ti) sphere in the presence of a pH 7.5 aqueous buffer. The Ti sphere also served as a conductive electrode for applying electricity to the adhesive, while a platinum (Pt) wire served as the counter electrode. Work of adhesion (W_{adh}) decreased with increased levels of applied voltage and current, exposure time to the applied electricity, and salt concentration of the interfacial buffer. Application of 9 V for 1 min completely deactivated the adhesive. UV-Vis diffuse reflectance spectra and tracking of catechol oxidation byproduct, hydrogen peroxide, confirmed that catechol was oxidized as a result of applied electricity. Contact mechanics testing further confirmed that the Young's modulus of the adhesive increased by nearly 4 folds at the interface as a result of oxidative crosslinking, even though the modulus of the bulk of the adhesive was unaffected by applied electricity. The accumulation of hydroxyl ions near the cathode increased the local solution pH, which promoted oxidation-induced crosslinking of catechol and subsequently decreased its adhesive property. Tuning adhesive properties through in-situ electrochemical oxidation provides on-demand control over the adhesive, which will potentially add another dimension in designing synthetic mimics of mussel adhesive proteins.

Graphical Abstract

*Corresponding Author Bruce P. Lee. bplee@mtu.edu.

ASSOCIATED CONTENT

The Supporting information is available free of charge via the http://pubs.acs.org

• Experimental details and additional data and figures

The authors declare no competing financial interest.

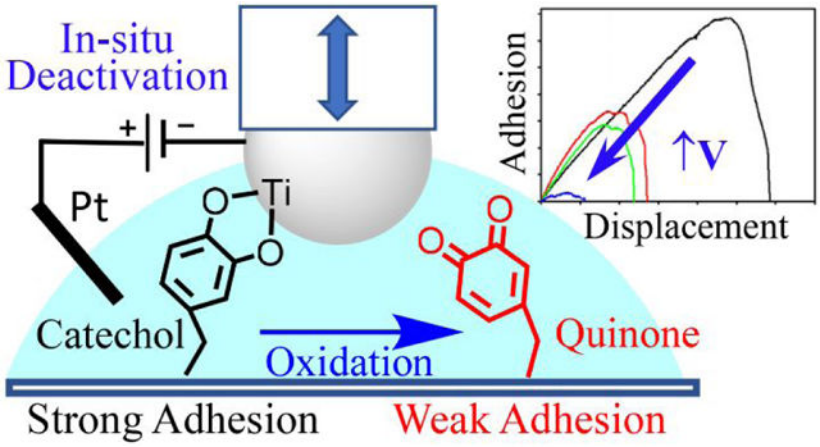

Keywords

Catechol-containing adhesive; Wet adhesion; In-situ deactivation; Electrochemical oxidation; Water electrolysis; JKR contact mechanics

Introduction:

A smart adhesive can be activated or deactivated in response to externally applied stimuli. Smart adhesives are of great interest for various applications in the biomedical field (e.g., painless removal of wound dressing[1-2] and prosthetics limb attachment with tissue[3-4]), various industries (e.g., on-demand attachment or detachment of components in the automotive industry[5-7] and structural joints[8-9]), and the manufacturing sectors. However, most of the existing smart adhesives are designed to adhere to dry surfaces and have limited adhesion to wet surfaces[10]. Therefore, a smart adhesive that can form strong adhesion to wet surfaces with tunable adhesive properties is in great demand.

To design a wet adhesive, researchers have taken an interest in underwater living creatures that can attach themselves firmly to wet surfaces, such as marine mussels[11-12], barnacles[13], sandcastle worms[14], and octopi[15]. Among these biomimetic strategies, our interest is in mussel-inspired wet adhesion. Marine mussels secret protein-based adhesives that contain a unique amino acid, 3,4-dihydroxyphenylalanine (DOPA). The catechol side chain of DOPA is responsible for strong adhesion to various underwater surfaces[16-18]. Many catechol-functionalized adhesives and coatings have been developed in the last decade for different applications ranging from multifunctional coatings[19] to skin wound closure[20], hemostatic agent[21], and drug delivery application[22]. Recently, catechol-containing smart adhesives that are responsive to light irradiation[23], change in temperature[24], or enzyme[25] have been reported. Similarly, our previous work demonstrated that pH can be used to modulate the interfacial binding property of catechol-based smart adhesives, by controlling the oxidation state of catechol[26-28]. The reduced form of catechol exhibits strong interfacial binding strength to inorganic substrates. The reported interfacial binding strength between the reduced form of catechol and a titanium (Ti) substrate averaged around 800 pN, which is 40% that of a covalent bond[29]. Catechol forms monodentate or bidentate coordination bonds

with Ti[30]. This binding strength is drastically reduced to 180 pN as a result of pH-induced oxidation of catechol[29]. However, using change in pH as an externally applied stimulus is limited by the slow diffusion of ions into the adhesive network and is highly impractical.

An alternative approach to tune the oxidation state of catechol is through electrochemical oxidation. Various studies have demonstrated the electrochemical oxidation of soluble catechol derivatives using cyclic voltammetry technique in a three-electrode electrochemical cell[31-33]. Electrochemical-induced oxidation and curing of catechol-containing adhesive was only demonstrated very recently[34-35]. Also, tuning the oxidation state of catechol by electrochemistry was used in controlling the movement of a hydrogel actuator[36]. Additionally, direct electrochemical oxidation of catechol-functionalized coatings was used to promote cell attachment and peptide immobilization through oxidation-induced crosslinking[37-38]. However, to our knowledge, there is no direct evidence that correlated the effect of in-situ electrochemical oxidation on the adhesive property of catechol.

Here, we tested the feasibility of deactivating the adhesive property of catechol by in-situ electrochemical oxidation, when the adhesive is in direct contact with a surface substrate (Scheme 1). Johnson-Kendall-Roberts (JKR) contact mechanics test was used to evaluate changes in the interfacial binding property of catechol-containing adhesive with a Ti sphere in the presence of an interfacial buffer solution (pH 7.5) (Figure 1). The Ti sphere also served as a conductive electrode for applying electricity to the adhesive, while a platinum (Pt) wire was utilized as the counter electrode. The effect of applied voltage and current levels, exposure time, and salt concentration of the interfacial buffer on the adhesive property of catechol was determined. Electrochemical oxidation of catechol was confirmed using UV-Vis diffuse reflectance spectroscopy and tracking the production of hydrogen peroxide (H_2O_2), a byproduct generated during catechol oxidation[39]. Finally, contact mechanics testing and oscillatory rheometry were performed to determine the effect of applied electricity on the mechanical properties at the interface and in the bulk of the adhesive, respectively.

Results:

The model adhesive used in the experiment consisted of 10 mol% dopamine methacrylamide (DMA, Figure S1) copolymerized with methoxyethyl methacrylate (MEA) and 3 mol% methylene bis-acrylamide (MBAA) as the crosslinker (Figure S2). DMA consists of a catechol moiety linked to a polymerizable monomer. DMA remained redox active and exhibited similar anodic and cathodic peaks associated with the formation of semiquinone and quinone that were also found in N-acetyldopamine based on cyclic voltammetry experiments (Figure S3). FTIR spectra confirmed the presence of catechol (−OH 3383 cm^{-1} and benzene rings 1486, 1583, and 1609 cm^{-1}) in the adhesive (Figure S4).

In a typical JKR contact mechanics test, the Ti sphere was brought into contact with the adhesive wetted with 200 μL of pH 7.5 Tris buffer containing 0.1 M NaCl. The Ti sphere was compressed at 1 μm/s until a maximum preload of 10 mN was reached and then retracted at the same speed (Figure S5). In the absence of applied electricity, the virgin adhesive exhibited a maximum tensile load of nearly 70 mN despite a preload of only 10

mN (Figure 2a). This indicated that catechol contributed to strong interfacial binding in the presence of water. To determine the effect of in-situ applied electrical filed on adhesion, up to 9 V was applied to the adhesive using the Ti sphere as the cathode and a Pt wire as the anode while the Ti sphere was still in direct contact with the adhesive. The interfacial binding properties of the adhesive decreased significantly with increased levels of applied voltage. The work and strength of adhesion (W_{adh} and S_{adh}, respectively) decreased by 96% and nearly 100%, respectively, at the highest voltage tested (9 V) when compared to the virgin adhesive (Figure 2b-c). S_{adh} decreased near linearly with increased applied voltage in the range of 1 to 5V (Figure S6). Adhesives oxidized by incubation in a pH 9 solution also exhibited nearly zero adhesive properties (Figure S7), confirming that the reduced form of catechol is responsible for strong wet adhesion. As expected, the measured current increased with increased applied voltage (Figure 2d).

The images of catechol-containing adhesive after exposure to applied voltage can be found in Figure S8 a-c. The surface of the adhesive surrounding the cathode (Ti sphere) appeared red in color, an indication of catechol oxidation[40]. With increasing applied voltage, this localized color change increased in surface area. On the other hand, the surface of the adhesive remained white near the anode (Pt wire). Litmus paper was used to determine the change in solution pH near each electrode. The solution near the cathode became basic (green color; pH ~ 10.0 for 9 V), whereas the solution became acidic (orange color; pH ~ 3.0) near the anode. Samples that did not contain catechol remained white, even though the litmus paper indicated similar pH changes in the interfacial liquid after the application of voltage (Figure S8 d-f).

Elevated applied voltage likely resulted in electrolysis of water (Scheme 2), which produced gaseous oxygen (O_2 (g)) and proton ion (H^+) near the anode (Pt) and gaseous hydrogen (H_2 (g)) and hydroxyl ion (OH^-) near the cathode (Ti)[41]. Generation of O_2 (g) and H_2 (g) results in bubble formation near the electrodes, which can cause the measured current to fluctuate[42-43]. Current fluctuation was clearly visible with an applied voltage of 9 V (Figure 2d). Accumulation of OH^- near the Ti sphere and H^+ near the Pt wire changed the local solution pH[44-48]. Increased level of local solution pH near the Ti sphere promoted catechol oxidation and subsequently decreased the measured adhesive property. The interfacial buffer contained 0.1 M NaCl. The oxidation of chloride ions to chlorine gas (Cl_2 (g)) occurred near the anode[49] and would have minimal impact on the interfacial binding between Ti (cathode) and catechol.

To confirm catechol oxidation, UV-Vis diffuse reflectance spectra of catechol-containing adhesive was obtained (Figure 3a). Catechol-containing adhesives exhibited a broad peak (400–600 nm) after exposure to elevated levels of applied voltage (5 and 9 V). Samples oxidized by incubation in a pH 9 solution also exhibited a broad peak in the same range of wavelength. This peak can be attributed to the oxidation products of catechol such as quinone as well as the dimers formed from oxidative crosslinking of catechol[50]. The adhesives exposed to 1 V did not exhibit a similar peak potentially due to the reduced level of localized oxidation. Adhesives treated with a pH 3 solution exhibited increased reflectance at a wavelength lower than 400 nm due to the presence of catechol (λ_{max} = 280 nm)[50].

The concentration of H_2O_2 in the interfacial Tris buffer solution was determined to further confirm the oxidation of catechol. H_2O_2 is a byproduct generated during catechol oxidation (Figure S9)[39]. The measured concentration of H_2O_2 increased with increasing applied voltage and exposure time (Figure 3b), which is indicative of an increased level of catechol oxidation. The highest amount of H_2O_2 was measured for the adhesive exposed to 9 V for 2 min (45 μM). Without any applied voltage (0 V), no H_2O_2 was generated from the adhesive. When electrical potential was applied to the interfacial buffer in the absence of the adhesive, a small amount of H_2O_2 was detected and the concentration increased with increasing applied voltage (Figure S10). H_2O_2 could be generated due to the reduction of O_2 (g) or the combination of H_2 (g) and O_2 (g)[51-52]. However, the amount of H_2O_2 generated by the electrolysis of water was significantly lower than the amount generated by electrochemical oxidation of catechol.

Contact mechanics tests and oscillatory rheometry experiments were performed to investigate the effect of electrochemical oxidation on the mechanical properties at the interface and within the bulk of the adhesive, respectively, after the application of electricity. The contact curves (Figure S11) were fitted with the Hertzian model (Equation S8) to determine the Young's modulus of the adhesive at the interface (E_{inf}) [53]. E_{inf} increased with increased applied voltage (Table S1). At the highest voltage level (9 V for 1 min), E_{inf} reached 76 kPa, which is nearly 4 folds higher when compared to that of the virgin adhesive (E_{inf} = 20 kPa). On the contrary, the storage modulus (G') remained around 4 – 5 kPa for all samples (Figure S12). This indicated that the overall stiffness of the adhesive did not change and the increase in stiffness occurred only at the interface. Cross-sectional views of the adhesive samples also confirmed that oxidation (red color) occurred only near the interface (Figure S13), with a maximum depth of around 0.2 mm from the surface of the adhesive treated with 9 V. Additionally, adhesive property measured on the opposite side of the oxidized surface was not affected by the electrochemical treatment (Figure S14). These results collectively indicated that oxidation occurred mainly at the interface where electrochemical oxidation took place.

Electrochemical oxidation-induced catechol crosslinking was further confirmed using a model linear copolymer, p(DMA-co-MEA) (Figure S15). Fourier-transform infrared spectroscopy-attenuated total reflection (FTIR-ATR) spectrum of p(DMA-co-MEA) exhibited three peaks at 813, 782, and 754 cm^{-1} (Figure S16), which were attributed to the C-H bending of the aromatic ring[54]. The intensity of these peaks reduced with increased level of applied voltage, potentially due to the oxidative crosslinking of catechol. Additionally, p(DMA-co-MEA) was initially soluble in both aqueous and various organic solvents (e.g., tetrahydrofuran, dimethyl sulfoxide, and chloroform) and became insoluble in these solvents after electrochemical treatment (Figure S17), potentially due to chemical crosslinking of catechol. ^{1}H NMR spectra of *N*-acetyldopamine also confirmed catechol crosslinking. After electrochemical treatment (9V for 1 min), the peaks associated with the aromatic protons became broad in shape as opposed to sharp peaks found in the unoxidized *N*-acetyldopamine (Figure S18). This result indicated that oxidative crosslinking and polymerization of the catechol had occurred[55]. Oxidized catechol is highly reactive and can irreversibly crosslink to form oligomers consisted of up to 6 catechol residues[56].

The temperature of interfacial buffer increased by only 1.22 ± 0.1 °C during electrochemical treatment using the highest applied voltage of 9 V (Figure S19). The increase in temperature was relatively low, potentially due to the high specific heat of water. Although we have previously demonstrated that the rate of catechol oxidation increases at an elevated temperature[39], the small increase in temperature associated with electrochemical treatment likely had a minimal effect on catechol oxidation.

Three supplementary videos captured the in-situ deactivation of the adhesive as a result of applied electrical potential (Supplementary Videos 1-3). A 1-g weight consisted of the Ti sphere and the indenter shaft was attached to the adhesive in the presence of interfacial buffer, in a setup that resembles the inverted JKR testing condition. A green light-emitting diode (LED) was attached in series with the electrodes and the source meter, which served as an indicator when the current was passing through the adhesive joint. The LED light turned off when the weight was detached. When a voltage of 9 V was applied, the weight detached within 7 sec. The detachment of the weight occurred due to a decrease in adhesive strength to the extent that the adhesive could no longer support the weight. When a lower voltage was applied, a significantly longer amount of time was required to deactivate the adhesive (23 sec and 2 min 23 sec for 5 and 1 V, respectively). These videos corroborate with JKR contact mechanics test results where higher applied voltage resulted in a larger decrease in adhesive property (Figure 2).

JKR contact mechanics test was also performed using the adhesive-contacting Ti sphere as the anode and the Pt wire as the cathode. Although both W_{adh} and S_{adh} values decreased with increasing applied voltage (Figure 4 and Figure S20), the extent of decrease in these values was significantly lower (~50% reduction at 9 V) when compared to adhesion tests performed using Ti sphere as the cathode (>96% reduction at 9 V; Figure 2). The anodic Ti oxidized catechol, which resulted in decreased adhesion. However, the anodic reaction associated with electrolysis of water also generated H^+ and acidified the solution surrounding the anode[41], which counteracted catechol oxidation. Cl_2 can also be generated near the anode from chloride ion, which can be further transformed into hypochlorite, chlorite, chlorate, or perchlorate ions.[57] These ions can potentially reduce the solution pH and counteract catechol oxidation. The photographs of the adhesive confirmed pH-induced oxidation near the cathodic Pt wire (red color) while the surface of the adhesive near the anodic Ti sphere only exhibited slight discoloration (Figure S8 g-i). UV-Vis diffuse reflectance spectra also did not exhibit similar peaks (400 – 600 nm) associated with pH-oxidized catechol (Figure S21). Given that using a cathodic Ti sphere as a contacting surface more effectively oxidized catechol and deactivated its adhesive property, subsequent experiments were performed using Ti as the cathode.

In addition to varying the level of the applied electrical potential, the effect of other factors such as applied current level, exposure time, salt concentration of the interfacial buffer, and catechol concentration on adhesion was also investigated. Up to 10 mA of current was applied to DMA-containing adhesive. Both W_{adh} and S_{adh} decreased with increased level of electrical current application (Figure S22). As expected, the measured voltage across two electrodes increased with increased applied current (Figure S22d). When the adhesive was exposed to increased length of exposure to 5 V of electrical potential, the interfacial binding

properties of the adhesive also decreased with increasing length of exposure to the electrical field (Figure S23). At the highest exposure time of 2 min, W_{adh} and S_{adh} values were reduced by 86% and 64%, respectively, when compared to the virgin adhesive (Figure S23). Similarly, increasing NaCl concentration in the interfacial buffer from 0.1 M to 1 M also resulted in further decreased adhesion as a result of increased conductivity in the adhesive joint as indicated by an increase in the measured current (Figure S24). Regardless of the treatment, the decrease in adhesion property was accompanied by an increased extent of catechol oxidation as indicated by an increased area of localized color change (red color) on the sample surface (Figures S22 e-g, S23 d-f, and S24 e-g). Finally, adhesives were prepared with varying DMA concentration (5 to 15 mol%). For the virgin adhesive, both W_{adh} and S_{adh} increased with increasing catechol content, indicating that catechol is responsible for strong interfacial binding in the presence of an aqueous solution (Figure S25). After electrochemical treatment (5 V for 1 min), both W_{adh} and S_{adh} decreased by 55-65% and 60-85%, respectively, when compared to the virgin adhesive.

To evaluate whether the electrochemically oxidized catechol can be converted back to its adhesive and reduced form, DMA-containing adhesive was incubated in a pH 3 solution for 24 h after electrochemical treatment. Based on JKR contact mechanics test (Table S2), pH 3 treated adhesive did not demonstrate a recovery in its adhesive property. On the contrary, the measured adhesion values decreased further. This is potentially due to the continued oxidation of catechol by the basic solution that was trapped within the adhesive network. Similar observation has been previously reported in pH-induced oxidation of catechol-containing adhesive[26]. UV-vis diffuse reflectance spectra (Figure 3a), FTIR-ATR of p(DMA-co-MEA) (Figure S16), ^{1}H NMR of *N*-acetayldopamine (Figure S18) and increase in E_{inf} (Table S1) collectively suggested that irreversible oxidative crosslinking had occurred, which potentially limited the reversibility of catechol.

Discussion:

Taken together, this work demonstrated for the first time that it is feasible to directly deactivate catechol-containing adhesive by in-situ electrochemical oxidation. Electrolysis of water increased the solution pH near the cathode, which resulted in catechol oxidation (Scheme 2). In an oxygenated aqueous solution, catechol readily oxidizes in a basic solution (pKa = 9.2 and 14 for catechol)[58]. Catechol oxidation occurred even when the adhesive was bound to a surface substrate. While it is possible to deactivate catechol-containing adhesive using electrical potential as low as 1 V, elevated applied voltage was required to rapidly deactivate the adhesive. This is potentially due to the poor conductivity of the model adhesive network (0.57 S/m, Table S3). This requirement may be problematic due to the generation of side reaction products associated with electrolysis of water[41, 57, 59]. It may be necessary to increase the conductivity of the adhesive network to reduce the need for elevated electrical potential.

A custom-build JKR contact mechanics test setup was utilized to directly apply electricity to the adhesive joint. This setup enabled us to probe the interfacial interaction between the catechol-containing adhesive and Ti, while minimizing the contribution of the bulk property of the adhesive on the measured values. This differs from the oft-used lap shear adhesion

testing or peel test, where the bulk mechanical property plays a significant role in the measured adhesion values[60]. Additionally, we were able to characterize interfacial binding properties in the presence of water using a buffer solution of desired pH.

Elevated applied voltage likely resulted in irreversible crosslinking and the electrochemically oxidized catechol was unable to revert to its reduced and adhesive state. Catechol and the oxidized quinone can generate an aryloxy radical which leads to phenol coupling and dimer formation (Figure S27) [61-62]. A temporary protecting group such as a boronic acid, may be required to prevent catechol oxidation and crosslinking. Boronic acid forms pH dependent reversible complex with catechol and has been utilized in the synthesis of catechol-containing polymers[63]. Additionally, smart adhesives consisting of boronic acid and catechol demonstrated multiple cycles of reversible adhesion, due to the ability of boronic acid to protect catechol from irreversible oxidation at a basic pH[26-28].

Nevertheless, the ability to tune the adhesive property using applied electricity as the external trigger is highly attractive and convenient. An electro-responsive adhesive can potentially be integrated with electronic devices, which will offer users unprecedented control over the interfacial binding properties of the adhesive. In the Supplementary Videos, we demonstrated that it is feasible to deactivate adhesion with a simple “push of a button”. Additionally, there are very limited examples of smart adhesive that can bind to wet surfaces. Catechol is widely used to impart adhesive property to polymers with strong, wet adhesive property[11-12]. Although we had demonstrated in-situ deactivation using a model catechol-containing adhesive with an inert polyMEA backbone, it is potentially feasible to adopt the findings reported here to other catechol-based adhesives with a wide range of compositions and architectures.

Conclusion:

We developed a contact mechanics test setup to evaluate the effect of direct application of an electrical field on the adhesive property of catechol. Adhesive property of catechol-containing adhesive decreased with increased level of applied voltage and current, exposure time, and salt concentration of the interfacial buffer. From UV-Vis diffuse reflectance spectra and quantification of H_2O_2 generated at the interface, it was determined that in-situ electrochemical oxidation of catechol contributed to the decreased adhesive property. Electrochemical oxidation promoted catechol crosslinking and increased the Young’s modulus of adhesive near the interface of the adhesive. Catechol oxidation was confined to the interface and the stiffness within the bulk of the adhesive remained unchanged. Irreversible oxidative crosslinking of catechol limited the reversibility of inactivated catechol.

Supplementary Material

Refer to Web version on PubMed Central for supplementary material.

ACKNOWLEDGMENT

The authors acknowledge the Machine Shop of the Department of Manufacturing and Mechanical Engineering Technology at Michigan Technological University for helping in the preparation of PTFE indenter, and titanium spheres for the JKR contact mechanics test. The authors also acknowledge Jerry L. Lutz for assistance in using the Shimadzu 3600plus UV-vis spectrometer.

Funding Sources

This project was supported by the Office of Naval Research under award number N00014-16-1-2463 and the National Institutes of Health under award number R15GM104846.

REFERENCES

1. Kasprzak KA, Method for removing tacky adhesives and articles adhered therewith. Google Patents: 1982.
2. Coulthard P; Esposito M; Worthington HV; van der Elst M; van Waes OJ; Darcey J, Tissue adhesives for closure of surgical incisions. Cochrane Database Syst Rev 2010, (5).
3. Park J; Lee Y; Hong J; Ha M; Jung Y-D; Lim H; Kim SY; Ko H, Giant tunneling piezoresistance of composite elastomers with interlocked microdome arrays for ultrasensitive and multimodal electronic skins. ACS nano 2014, 8 (5), 4689–4697. [PubMed: 24592988]
4. Park J; Lee Y; Hong J; Lee Y; Ha M; Jung Y; Lim H; Kim SY; Ko H, Tactile-direction-sensitive and stretchable electronic skins based on human-skin-inspired interlocked microstructures. ACS nano 2014, 8 (12), 12020–12029. [PubMed: 25389631]
5. Banea M; da Silva LF; Carbas R; de Barros S, Debonding on command of multi-material adhesive joints. J ADHESION 2017, 93 (10), 756–770.
6. dos Reis M; Banea M; da Silva L; Carbas R, Mechanical characterization of a modern epoxy adhesive for automotive industry. Journal of the Brazilian Society of Mechanical Sciences and Engineering 2019, 41 (8), 340.
7. Machado J; Nunes P; Marques E; da Silva LF, Adhesive joints using aluminium and CFRP substrates tested at low and high temperatures under quasi-static and impact conditions for the automotive industry. Compos. B. Eng 2019, 158, 102–116.
8. Wang M; Song Q; Gu Y; Wu C; Liu J; Zhou X; Du M, Multiple high-temperature resistant phases modified phosphate-based adhesive for engineering ceramic connection in extreme environment. Ceram. Int 2019, 45 (1), 516–521.
9. Fernie JA; Drew R; Knowles K, Joining of engineering ceramics. Int. Mater. Rev 2009, 54 (5), 283–331.
10. Croll AB; Hosseini N; Bartlett MD, Switchable Adhesives for Multifunctional Interfaces. Advanced Materials Technologies 2019, 1900193.
11. Ahn BK, Perspectives on mussel-inspired wet adhesion. J. Am. Chem. Soc 2017, 139 (30), 10166–10171. [PubMed: 28657746]
12. Kord Forooshani P; Lee BP, Recent approaches in designing bioadhesive materials inspired by mussel adhesive protein. Journal of Polymer Science Part A: Polymer Chemistry 2017, 55 (1), 9–33.
13. So CR; Yates E; Estrella L; Schenck A; Yip C; Wahl KJ, Wet Adhesive Nanomaterials Inspired by the Barnacle Adhesive. Biophys. J 2018, 114 (3), 192a–193a.
14. Stewart RJ; Wang CS; Shao H, Complex coacervates as a foundation for synthetic underwater adhesives. Advances in colloid and interface science 2011, 167 (1-2), 85–93. [PubMed: 21081223]
15. Baik S; Park Y; Lee T-J; Bhang SH; Pang C, A wet-tolerant adhesive patch inspired by protuberances in suction cups of octopi. Nature 2017, 546 (7658), 396. [PubMed: 28617467]
16. Waite JH, Nature's underwater adhesive specialist. Int. J. Adhes. Adhes 1987, 7 (1), 9–14.
17. Lee BP; Messersmith PB; Israelachvili JN; Waite JH, Mussel-inspired adhesives and coatings. Annual review of materials research 2011, 41, 99–132.
18. Lu Q; Danner E; Waite JH; Israelachvili JN; Zeng H; Hwang DS, Adhesion of mussel foot proteins to different substrate surfaces. Journal of The Royal Society Interface 2013, 10 (79), 20120759.

19. Kang SM; Rho J; Choi IS; Messersmith PB; Lee H, Norepinephrine: material-independent, multifunctional surface modification reagent. Journal of the American Chemical Society 2009, 131 (37), 13224–13225. [PubMed: 19715340]
20. Han L; Yan L; Wang K; Fang L; Zhang H; Tang Y; Ding Y; Weng L-T; Xu J; Weng J, Tough, self-healable and tissue-adhesive hydrogel with tunable multifunctionality. NPG Asia Materials 2017, 9 (4), e372.
21. Ryu JH; Lee Y; Kong WH; Kim TG; Park TG; Lee H, Catechol-Functionalized Chitosan/Pluronic Hydrogels for Tissue Adhesives and Hemostatic Materials. Biomacromol. 2011, 12 (7), 2653–2659.
22. GhavamiNejad A; SamariKhalaj M; Aguilar LE; Park CH; Kim CS, pH/NIR light-controlled multidrug release via a mussel-inspired nanocomposite hydrogel for chemo-photothermal cancer therapy. Scientific reports 2016, 6, 33594. [PubMed: 27646591]
23. Shafiq Z; Cui J; Pastor-Pérez L; San Miguel V; Gropeanu RA; Serrano C; del Campo A, Bioinspired underwater bonding and debonding on demand. Angewandte Chemie International Edition 2012, 51 (18), 4332–4335. [PubMed: 22461306]
24. Zhao Y; Wu Y; Wang L; Zhang M; Chen X; Liu M; Fan J; Liu J; Zhou F; Wang Z, Bio-inspired reversible underwater adhesive. Nature communications 2017, 8 (1), 2218.
25. Wilke P; Helfricht N; Mark A; Papastavrou G; Faivre D; Börner HG, A direct biocombinatorial strategy toward next generation, mussel-glue inspired saltwater adhesives. Journal of the American Chemical Society 2014, 136 (36), 12667–12674. [PubMed: 25133879]
26. Narkar AR; Barker B; Clisch M; Jiang J; Lee BP, pH responsive and oxidation resistant wet adhesive based on reversible catechol–boronate complexation. Chemistry of Materials 2016, 28 (15), 5432–5439. [PubMed: 27551163]
27. Narkar AR; Lee BP, Incorporation of Anionic Monomer to Tune the Reversible Catechol-Boronate Complex for pH-Responsive, Reversible Adhesion. Langmuir 2018, 34 (32), 9410–9417. [PubMed: 30032614]
28. Narkar AR; Kendrick C; Bellur K; Leftwich T; Zhang Z; Lee BP, Rapidly responsive smart adhesive-coated micropillars utilizing catechol-boronate complexation chemistry. Soft matter 2019, 15 (27), 5474–5482. [PubMed: 31237299]
29. Lee H; Scherer NF; Messersmith PB, Single-molecule mechanics of mussel adhesion. Proceedings of the National Academy of Sciences 2006, 103 (35), 12999–13003.
30. Saiz-Poseu J; Mancebo-Aracil J; Nador F; Busqué F; Ruiz-Molina D, The Chemistry behind Catechol-Based Adhesion. Angewandte Chemie International Edition 2019, 58 (3), 696–714. [PubMed: 29573319]
31. Khalafi L; Rafiee M; Shahbak M; Shirmohammadi H, Kinetic Study of the Oxidation of Catechols in the Presence of N-Methylaniline. Journal of Chemistry 2013, 2013.
32. Kasa T; Solomon T, Cyclic Voltammetric and Electrochemical Simulation Studies on the Electro-Oxidation of Catechol in the Presence of 4, 4-bipyridine. American Journal of Physical Chemistry 2016, 5 (3), 45–55.
33. Robole ZM; Rahn KL; Lampkin BJ; Anand RK; VanVeller B, Tuning the Electrochemical Redox Potentials of Catechol with Boronic Acid Derivatives. The Journal of organic chemistry 2019, 84 (4), 2346–2350. [PubMed: 30681336]
34. Mou C; Ali F; Malaviya A; Bettinger CJ, Electrochemical-mediated gelation of catechol-bearing hydrogels based on multimodal crosslinking. Journal of Materials Chemistry B 2019, 7 (10), 1690–1696. [PubMed: 31372223]
35. Gan L; Tan NC; Gupta A; Singh M; Pokholenko O; Ghosh A; Zhang Z; Li S; Steele TW, Self curing and voltage activated catechol adhesives. Chemical Communications 2019, 55 (68), 10076–10079. [PubMed: 31378790]
36. Xue B; Qin M; Wang T; Wu J; Luo D; Jiang Q; Li Y; Cao Y; Wang W, Electrically controllable actuators based on supramolecular peptide hydrogels. Advanced Functional Materials 2016, 26 (48), 9053–9062.
37. Furst AL; Smith MJ; Francis MB, Direct electrochemical bioconjugation on metal surfaces. JACS 2017, 139 (36), 12610–12616.

38. Li J; Sun C-L; Shen R; Cao X-Y; Zhou B; Bai D-C; Zhang H-L, An Electrochemically Switched Smart Surface for Peptide Immobilization and Conformation Control. JACS 2014, 136 (31), 11050–11056.
39. Meng H; Forooshani PK; Joshi PU; Osborne J; Mi X; Meingast C; Pinnaratip R; Kelley J; Narkar A; He W, Biomimetic recyclable microgels for on-demand generation of hydrogen peroxide and antipathogenic application. Acta biomaterialia 2019, 83, 109–118. [PubMed: 30541699]
40. Narkar AR; Kelley JD; Pinnaratip R; Lee BP, Effect of Ionic Functional Groups on the Oxidation State and Interfacial Binding Property of Catechol-Based Adhesive. Biomacromol. 2018, 19 (5), 1416–1424.
41. Hou M; Chen L; Guo Z; Dong X; Wang Y; Xia Y, A clean and membrane-free chlor-alkali process with decoupled Cl 2 and H 2/NaOH production. Nature communications 2018, 9 (1), 438.
42. Mazloomi S; Sulaiman N, Influencing factors of water electrolysis electrical efficiency. Renewable and Sustainable Energy Reviews 2012, 16 (6), 4257–4263.
43. Yang X; Baczyzmalski D; Cierpka C; Mutschke G; Eckert K, Marangoni convection at electrogenerated hydrogen bubbles. PCCP 2018, 20 (17), 11542–11548. [PubMed: 29651493]
44. Marini S; Salvi P; Nelli P; Pesenti R; Villa M; Berrettoni M; Zangari G; Kiros Y, Advanced alkaline water electrolysis. Electrochim. Acta 2012, 82, 384–391.
45. Kuila T; Bose S; Khanra P; Mishra AK; Kim NH; Lee JH, Recent advances in graphene-based biosensors. Biosens. Bioelectron 2011, 26 (12), 4637–4648. [PubMed: 21683572]
46. Zeng K; Zhang D, Recent progress in alkaline water electrolysis for hydrogen production and applications. Progress in Energy and Combustion Science 2010, 36 (3), 307–326.
47. Santos DM; Sequeira CA; Figueiredo JL, Hydrogen production by alkaline water electrolysis. Quim. Nova 2013, 36 (8), 1176–1193.
48. Wang M; Wang Z; Gong X; Guo Z, The intensification technologies to water electrolysis for hydrogen production–a review. Renewable and Sustainable Energy Reviews 2014, 29, 573–588.
49. Wang X; Teichgraeber H; Palazoglu A; El-Farra NH, An economic receding horizon optimization approach for energy management in the chlor-alkali process with hybrid renewable energy generation. Journal of Process Control 2014, 24 (8), 1318–1327.
50. Cencer M; Murley M; Liu Y; Lee BP, Effect of nitro-functionalization on the cross-linking and bioadhesion of biomimetic adhesive moiety. Biomacromolecules 2014, 16 (1), 404–410. [PubMed: 25495043]
51. Drogui P; Elmaleh S; Rumeau M; Bernard C; Rambaud A, Hydrogen peroxide production by water electrolysis: application to disinfection. J. Appl. Electrochem 2001, 31 (8), 877–882.
52. Yuan S; Fan Y; Zhang Y; Tong M; Liao P, Pd-catalytic in situ generation of H2O2 from H2 and O2 produced by water electrolysis for the efficient electro-Fenton degradation of rhodamine B. Environ. Sci. Technol 2011, 45 (19), 8514–8520. [PubMed: 21866953]
53. Shull KR, Contact mechanics and the adhesion of soft solids. Materials Science and Engineering: R: Reports 2002, 36 (1), 1–45.
54. Trivedi MK; Branton A; Trivedi D; Nayak G, Characterization of physical, spectroscopic and thermal properties of biofield treated biphenyl. Am. J. Chem. Eng 2015, 3 (5), 58–65.
55. Liu Y; Meng H; Qian Z; Fan N; Choi W; Zhao F; Lee BP, A moldable nanocomposite hydrogel composed of a Mussel-inspired polymer and a nanosilicate as a fit-to-shape tissue sealant. Angewandte Chemie International Edition 2017, 56 (15), 4224–4228. [PubMed: 28296024]
56. Lee BP; Dalsin JL; Messersmith PB, Synthesis and gelation of DOPA-modified poly (ethylene glycol) hydrogels. Biomacromolecules 2002, 3 (5), 1038–1047. [PubMed: 12217051]
57. Czarnetzki L; Janssen L, Formation of hypochlorite, chlorate and oxygen during NaCl electrolysis from alkaline solutions at an RuO 2/TiO 2 anode. Journal of Applied Electrochemistry 1992, 22 (4), 315–324.
58. Nurchi VM; Pivetta T; Lachowicz JI; Crisponi G, Effect of substituents on complex stability aimed at designing new iron (III) and aluminum (III) chelators. Journal of inorganic biochemistry 2009, 103 (2), 227–236. [PubMed: 19036454]
59. Zhou W; Rajic L; Chen L; Kou K; Ding Y; Meng X; Wang Y; Mulaw B; Gao J; Qin Y, Activated carbon as effective cathode material in iron-free Electro-Fenton process: Integrated H2O2

electrogeneration, activation, and pollutants adsorption. Electrochimica acta 2019, 296, 317–326. [PubMed: 30631212]

60. Zhang W; Wang R; Sun Z; Zhu X; Zhao Q; Zhang T; Cholewinski A; Yang FK; Zhao B; Pinnaratip R, Catechol-functionalized hydrogels: biomimetic design, adhesion mechanism, and biomedical applications. Chemical Society Reviews 2020, 49, 433–464.
61. McDowell LM; Burzio LA; Waite JH; Schaefer J, Rotational echo double resonance detection of crosslinks formed in mussel byssus under high-flow stress. J. Biol. Chem 1999, 274 (29), 20293–5. [PubMed: 10400649]
62. Cencer MM; Liu Y; Winter A; Murley M; Meng H; Lee BP, Effect of pH on the rate of curing and bioadhesive properties of dopamine functionalized poly(ethylene glycol) hydrogels. Biomacromol. 2014, 15 (8), 2861–2869.
63. Huang K; Lee BP; Ingram DR; Messersmith PB, Synthesis and characterization of self-assembling block copolymers containing bioadhesive end groups. Biomacromolecules 2002, 3 (2), 397–406. [PubMed: 11888328]

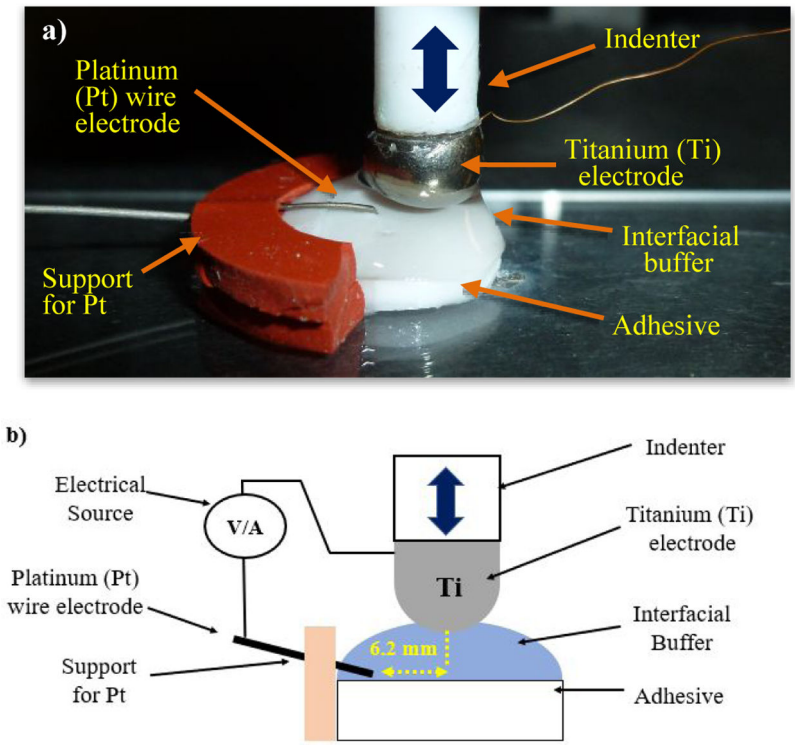

Figure 1:

(a) Photograph and (b) schematic representation of custom-built JKR contact mechanics setup used for adhesion testing and in-situ electrochemical oxidation.

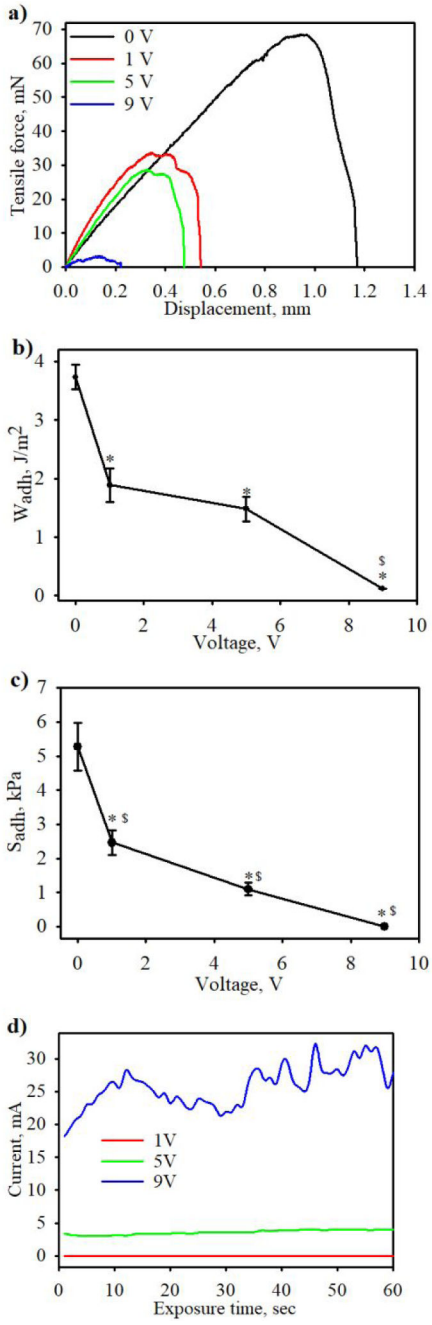

Figure 2:

(a) Typical JKR contact curves, (b) W_{adh}, (c) S_{adh}, and (d) recorded current for JKR contact mechanics testing performed with in-situ application of voltage for 1 min. Voltage was applied using a Ti sphere and a Pt wire as a cathode and an anode, respectively, in the presence of an interfacial buffer (pH 7.5). * $p < 0.05$ when compared to the virgin adhesive (0 V). $ $p < 0.05$ when compared to all other group.

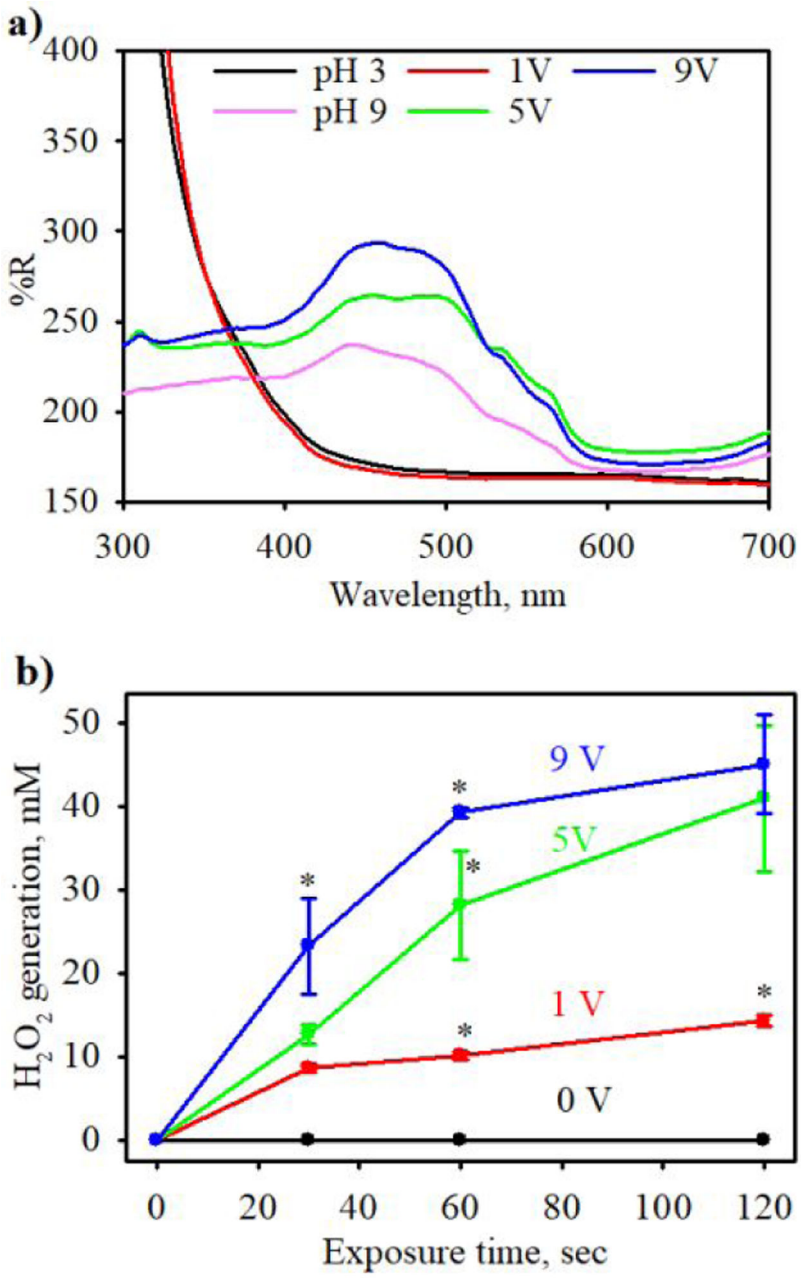

Figure 3:

(a) UV-vis diffuse reflectance spectra of freeze-dried adhesives after exposure to applied electrical potential. For comparison purposes, samples were immersed in either pH 3 or 9 solutions for 24 h to determine the spectra for the adhesive in the reduced (pH 3) and oxidized (pH 9) forms. (b) H_2O_2 concentration in the interfacial Tris buffer during in-situ application of voltage. * $p < 0.05$ when compared to other adhesives tested at same exposure time.

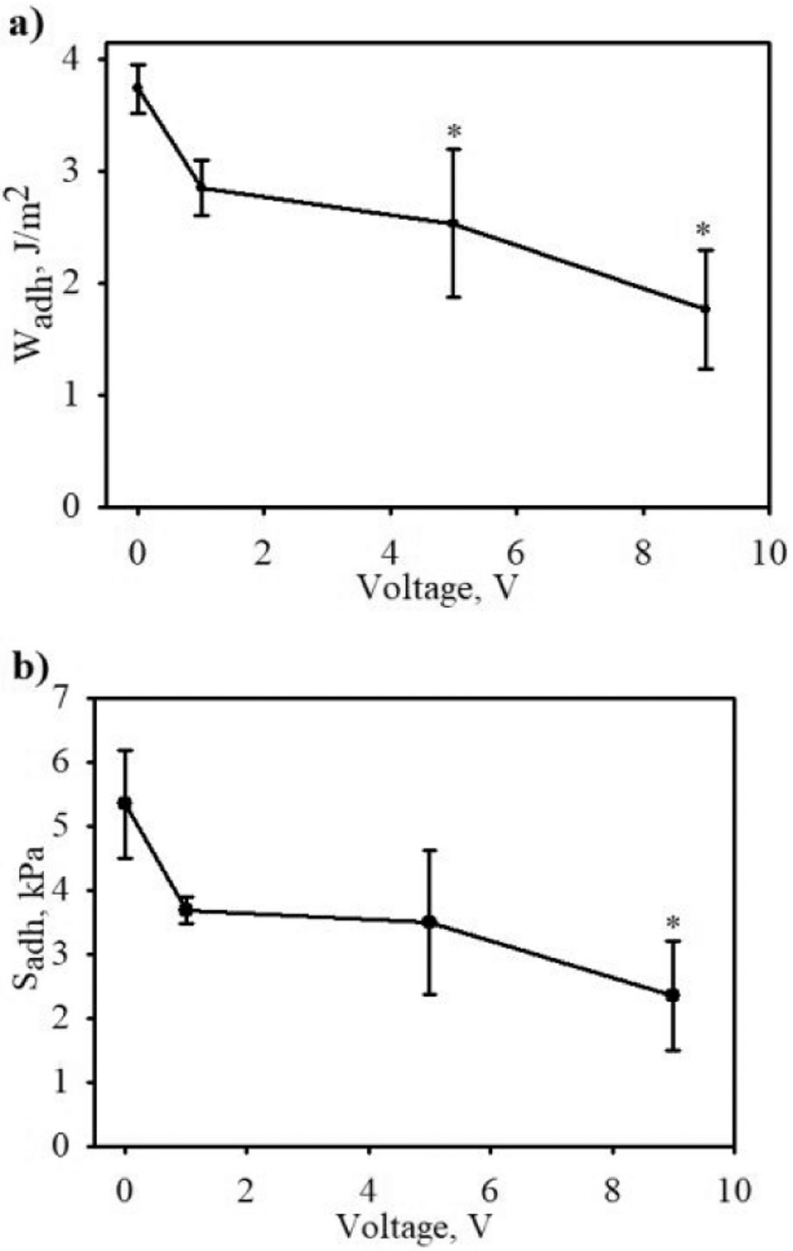

Figure 4:

(a) W_{adh} and (b) S_{adh} of catechol-containing adhesive tested with in-situ application of voltage for 1 min, using Ti sphere as the anode and Pt wire as the cathode, in the presence of an interfacial buffer (pH 7.5). * $p < 0.05$ when compared to the virgin adhesive (0 V).

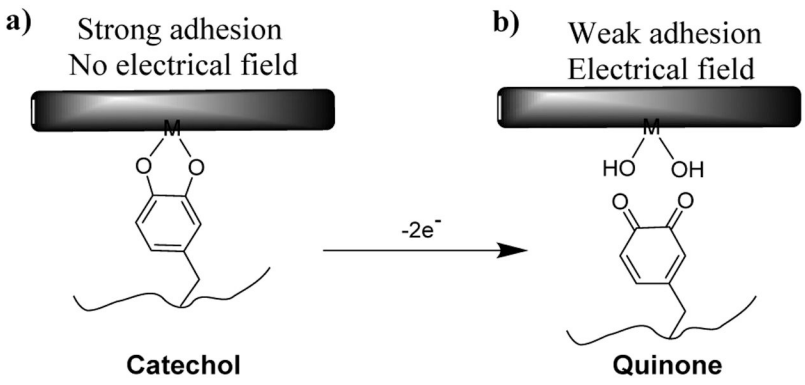

Scheme 1:

(a) The reduced form of catechol exhibits strong adhesion to metal surface in the absence of applied electrical field and (b) in-situ electrical application oxidizes catechol to its quinone form, which exhibits weak adhesion.

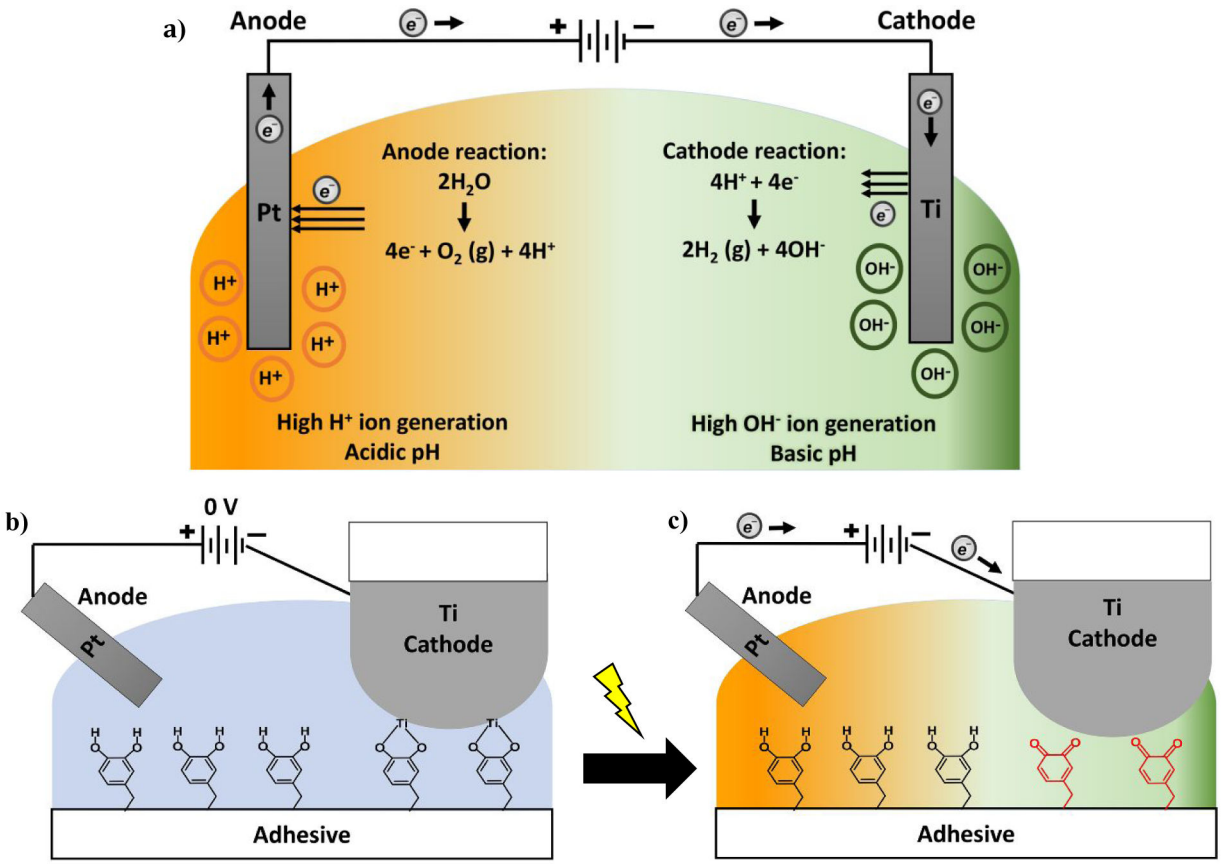

Scheme 2:

Schematic representation of the proposed mechanism of in-situ deactivation of catechol-containing adhesive. (a) The application of the electrical field initiates water electrolysis, which produced hydrogen (H_2 (g)) and hydroxyl ion (OH^-) near the cathode (Ti) and oxygen (O_2 (g)) and proton ion (H^+) near the anode (Pt). Accumulation of OH^- near the Ti sphere and H^+ near the Pt wire change the local solution pH to basic and acidic, respectively. (b) Catechol demonstrates strong adhesion toward Ti surface when no electrical field was applied. (c) After the application of an electrical field, the solution near the cathode (Ti) becomes basic (green), which resulted in the oxidation of catechol to its quinone and poorly adhesive form. The solution near the anode (Pt) became acidic (orange).